Battery Energy Storage System Control for Mitigating PV Penetration Impact on Primary Frequency Control and State-of-Charge Recovery

Battery Energy Storage System Control for Mitigating PV Penetration Impact on Primary Frequency Control and State-of-Charge Recovery

Ujjwal Datta, Akhtar Kalam, and Juan Shi

Abstract—Increasing PV penetration significantly diminishes system inertia that affects systems' damping capability to regulate primary frequency control. Unlike wind turbine, PV energy system is incapable of providing under-frequency support because of no stored kinetic energy and could cause penalties for violating regulatory requirements. Therefore, a droop-type, lead-lag controlled Battery Energy Storage System (BESS) with a novel adaptive SOC recovery strategy is proposed in this paper to provide additional damping, enhance the inertial ability of the system with 18.18% PV penetration and which satisfy Australian National Electricity Market (NEM) regulatory requirements. The adaptive SOC recovery aims to maintain flexible battery SOC value according to load/PV generation forecast and comply with future events such as peak PV generation or lower PV output during the passing cloud periods. The proposed adaptive SOC strategy regulates SOC based on the value of charging current and moreover, adaptive SOC recovery does not affect the maximum SOC limit for the regular network event. Simulation results demonstrate BESS efficacy in mitigating the adverse inertial impact of PV and accomplishing mandatory grid requirements. Moreover, the proposed adaptive SOC recovery shows the flexibility of BESS for SOC management planning in accordance with future events forecast.

Index Terms—Battery energy storage system, primary frequency control, Lead-lag controller, maximum and adaptive SOC, voltage control.

I. INTRODUCTION

THE penetration of sustainable renewable energy sources (RES) has been growing steadily during the last decade and expected to have similar trend in the coming years. According to present installation scenarios, renewable capacity growth is expected to reach another 30% (1150GW) of the present estimation (920GW) by 2022 under an accelerated case and PV capacity is expected to have 59.6% growth [1]. Therefore, dynamic impacts of PV in transmission network need to consider and detailed analysis of PV on overall system frequency control is yet to be explored thoroughly. The replacement of synchronous generators with less/non-inertial and uncertain RES reduces total system inertia and hence, system stability will encounter critical challenges in providing fast frequency response when the system experiences power

imbalance. Insufficient capability for frequency support can raise severe issues in power system operation and control [2]. Number of publications on frequency challenges related to PV penetration in power system are available. Stability studies by the authors in [3]–[5] argued that reduction in inertia increases frequency oscillations of the system. In addition, authors in [5] indicated that higher PV penetration induces dramatic frequency oscillation beyond grid operating standards that potentially threatens uninterrupted load supply. Power oscillation damper [6], synchronous power controller [7], [8] and multiple-model adaptive control strategy [9] is adopted at PV terminal to damp out power system oscillations resulted from temporary power imbalances and maintain robust damping performance. A droop-type control [10], synthetic inertia control [11] and operating point lower than maximum power point (MPP) [12] are proposed to regulate PV power output and contribute in system frequency regulation. A comparative study carried out by the authors in [13] demonstrated that a combination of droop and inertia control performs better than the conventional MPP tracking, or discrete droop and inertia control. However, PV power output is curtailed by more than 50% to provide such over-frequency regulation. Moreover, whereas wind turbine can provide a certain level of under/over frequency regulation through the use of its stored kinetic energy [14], PV is incapable of providing under-frequency support as PV does not have any rotating masses i.e. stored energy. As NEM has a penalty policy for violating Frequency Control Ancillary Services constraints [15], hence the auxiliary energy source is needed to ensure frequency control within the regulatory constraints and avoid any penalties with the increased PV penetration.

BESS has proven to have great potential in providing primary frequency reserve in emergency situation to maintain grid requirements [16]. BESS and other auxiliary devices, namely, shunt capacitor and ultra-capacitor offers enhanced damping performance [17]. However, the study did not bring any insight on BESS sizing and battery SOC. Moreover, a very low PV penetration level (1%) is considered for comparative analysis which does not describe the severity of increased large-scale PV penetration [17]. The performance of BESS in controlling primary frequency is demonstrated in an islanded Microgrid [18] and small power system [19]. However, the study is bounded to small-scale power system [18], [19]; also no RES is considered in the system [16]. A lead-lag based BESS control is presented in [20], [21] for frequency control and oscillation damping, nevertheless, the studies did

not consider any SOC recovery strategy.

Most of the studies have not suggested any means of recovering battery SOC. The authors in [22] presented that SOC recovery strategy reduces regulation failure and thereby minimizes accumulated penalty cost. In [23]–[25], battery/supercapacitor SOC recovery is presented in microgrid and validated through an experimental setup. However, as SOC recovery is restored to the nominal value, this lacks the maximum utilization of available battery capacity. In consideration of such inadequacy, an adjustable SOC recovery is presented in [19], however, such a method reduces overall usable battery capacity as the authors suggested to limit the maximum and minimum SOC operating region as part of their adopted strategy.

In this paper, a droop-type and lead-lag controlled BESS with a novel SOC recovery strategy is proposed to participate in primary frequency control according to the NEM grid requirements with 18.18% PV penetration and avoid frequency violation during contingency periods to avoid unwanted penalty by the transmission/distribution system operator. In addition, exchanging energy during primary frequency control may not violate SOC limit but it can significantly reduce battery SOC. Therefore, in the proposed design, in addition to conventional maximum charging SOC limit, a new adaptive SOC recovery approach is proposed to recover flexible battery SOC without affecting SOC limit for network event and ensure availability of BESS energy for the next possible disturbance event. To evaluate the dynamic performance of the proposed droop-controlled BESS, a medium size power transmission system is selected and BESS competence is investigated. BESS installation location with optimal BESS converter sizing is suggested on a trial and error basis in the event of multiple studied contingencies.

II. FREQUENCY STABILITY REQUIREMENTS

Grid codes compatibility require sufficient damping capability through available headroom to increase generators' output or externally installed energy storage devices. The generating units are expected to produce supplementary active power (up-to its maximum generation capacity) for under-frequency event and reduce active power (droop-type) for over-frequency event. The frequency operating standard varies between countries, types of energy sources (conventional or renewable) and types of contingencies. In this research, operating standards by the Australian NEM are considered as the benchmark for evaluating grid performance under the studied contingency events. Without any contingencies, grid must be maintained within non-critical frequency deadband of 0.997-1.003pu at any operating point of time.

According to NEM, mandatory transient frequency boundary for generation or load event is 0.99-1.01pu for 15s and 0.997-1.003pu within 5 minutes whereas for network event the limit is 0.98-1.02pu for 15s, 0.99-1.01pu within 1 minute and to the non-critical region within 5 minutes [26] and non-critical region for voltage is 0.9-1.1pu [27]. The aforementioned frequency requirements are used as reference to design, identify suitable BESS location and converter sizing; and provide

needed power oscillation damping to guarantee grid code compatibility.

III. CONTROL METHOD

A. Primary frequency control and RES

To maintain nominal system frequency (within non-critical frequency operating region), generator should match the load demand constantly by compensating any temporary power mismatches using generator's stored kinetic energy [18]. Therefore, frequency response by the governor for n system can be defined as in (1):

$$\frac{df}{dt} = \frac{f_{ref}}{2\sum H_n}\Delta P_d \qquad (1)$$

where, $\Delta P_d = P_G - P_L$, ΔP_d is the change in power demand, P_G is the generated power, P_L is the load power demand, $\sum H_n$ is the sum of system inertia constant of all rotating machines and f_{ref} is the nominal frequency. With the increasing penetration of zero inertial PV and closing down of fossil fueled power plants, overall inertia reduces. Hence, conventional governor regulated frequency control may not successfully compensate power imbalances resulting from disturbance events such as varying PV output, network or load contingency if system inertia is not improved through alternative processes. Therefore, a new lead-lag controlled BESS is presented in this study, as shown in Fig 1 to increase system inertia constant, contribute in primary frequency control and mitigate adverse impact of PV penetration in the grid. The frequency response to power imbalances with incorporated BESS can be written as in (2) [19]:

$$\frac{df}{dt} = \frac{f_{ref}}{H_{bess} + 2\sum H_n}\Delta P_d \qquad (2)$$

where, H_{bess} is BESS inertia constant, D_1 and D_2 are the droop coefficient of generation system SG_1 and SG_2 respectively.
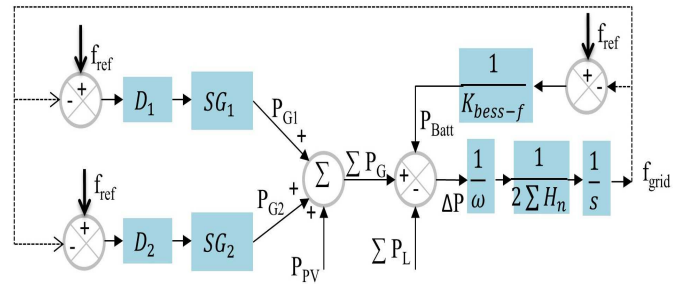

Fig. 1. Primary frequency control with BESS

The detailed model of the synchronous generators and BESS are discussed in [28] and in Section III-B, respectively.

B. The Overall Design of BESS and SOC Calculation

The general BESS diagram is shown in Fig. 2 that comprises a battery bank, bi-directional power conversion system and a suitable transformer to be connected with the grid. The BESS

converter control signals are frequency controller, voltage controller, active/reactive (PQ) controller, and charge controller. BESS converter operates according to the corresponding input reference signal and operating constraints of battery SOC. The detailed models of BESS are used to obtain simulation results and all the detailed system components of BESS including the battery model are presented throughout Sections III-B to III-E.
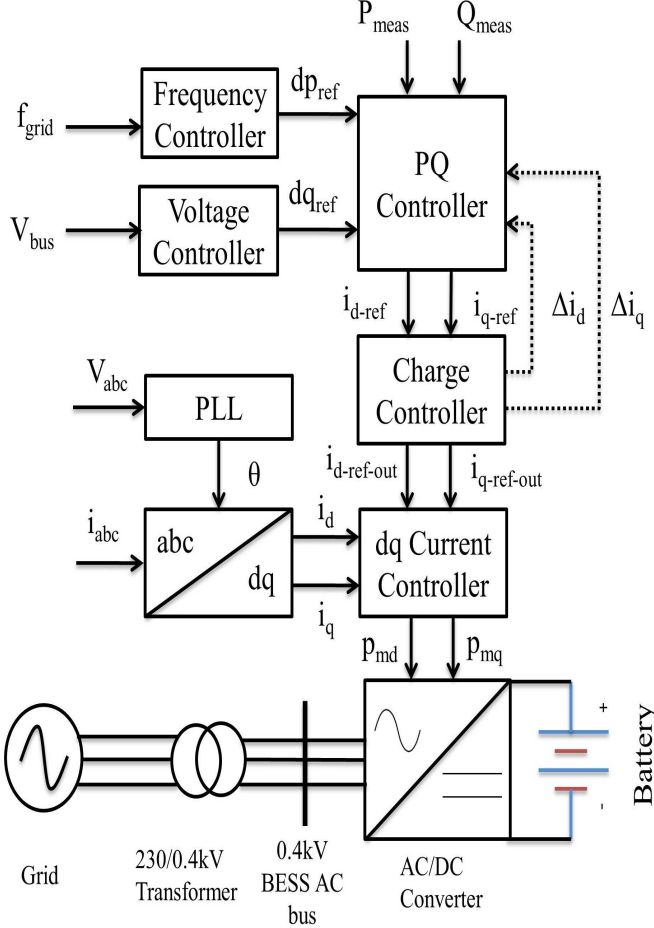

Fig. 2. Primary frequency control with BESS

The SOC calculation can be defined according to Coulomb counting method as in (3)

$$SOC_t = SOC_{t-1} + \int_{t-1}^{t} \frac{\eta\ I_{batt}}{3600\ C_{batt}}\ dt \qquad (3)$$

where, I_{batt} is the battery current, C_{batt} is the nominal battery capacity in ampere-hour (Ah), η is the Coulomb efficiency. It is understandable that battery efficiency may vary during the charging and discharging process differently in dynamic simulation studies and the assumption of lossless inverter may not be 100% accurate. However, a wide range of published research works have considered zero inverter losses i.e. the charging and discharging efficiencies are selected as 100% for SOC error analysis [29] and dynamic studies [23], [25], [30]–[32]. Considering the aforementioned established works, authors have chosen the value of Coulomb efficiency as 100% in this study.

State-of-health (SOH) is a measure of battery aging and is calculated as the ratio of current $vs.$ rated battery capacity. SOH of a new battery is considered as 100% and declines with the time of battery use. The current battery capacity is calculated using the change of Ah capacity and SOC. Nevertheless, SOH estimation is not a focus of this study and hence interested readers are suggested to read articles [33], [34] for the relevant information on SOH estimation.

Battery DC terminal voltage is 0.9kV whereas BESS AC side voltage is 0.4kV. BESS AC side is connected to the grid via a 0.4/230kV step-up transformer which provides the flexibility to be connected at different network voltages. The maximum charge voltage of each battery is 13.85V and there are 65 battery cells connected in parallel.

It is a challenging task to obtain an appropriate model that can symbolize the complex electrochemical and nonlinear nature of a battery. However, several attempts have been presented in the past to design an equivalent circuit to estimate battery response which is a simple R_{int} circuit [23], [25], [31], [34], [35] with less parameters and reasonable simplicity. The block diagram of R_{int} equivalent battery model for dynamic studies is shown in Fig. 3.
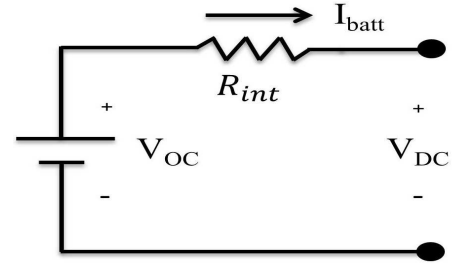

Fig. 3. Block diagram of R_{int} equivalent battery model

The battery is designed as a voltage source that depends on SOC with internal output resistance (R_{int}) which can be estimated as in (4) [36]:

$$V_{DC} = V_{max}\ SOC + V_{min}(1 - SOC) - I_{batt}\ R_{int} \qquad (4)$$

C. BESS Damping Controller with Feedback Signals

Substantial damping support is required to effectively minimize power system oscillations in the event of unexpected transient events. The control loop that generates necessary reference signals for BESS to contribute in damping control is shown in Figs. 4 and 5. Since wide area measurement is not used, the local measurements for voltage and frequency are used as input to regulate active and reactive power of BESS.

1) Frequency droop controller: The power-frequency droop is greatly affected with reduced system inertia and thereby influence significantly on power system stability. The basic concept of the adopted droop control is shown in Fig. 6 and the typical droop characteristics [37] can be written as in (5):

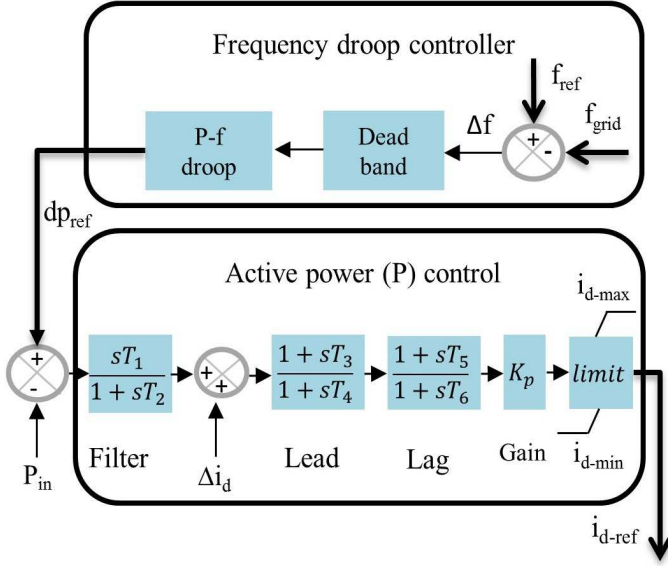$$dp_{ref} = \frac{1}{K_{bess-f}}(f_{ref} - f_{grid}) \qquad (5)$$

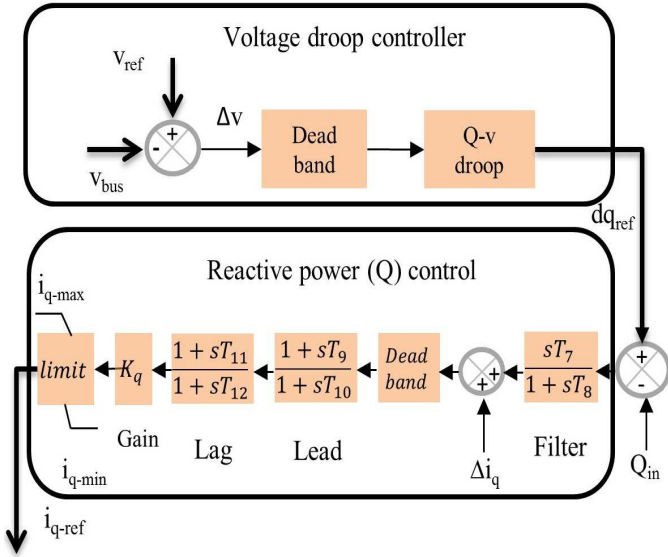Fig. 4. The block diagram of frequency and BESS active power control

Fig. 5. The block diagram of voltage and BESS reactive power control

where, f_{ref} is the frequency reference (1pu), dp_{ref} is the active power reference based on power-frequency (P-f) droop controller, K_{bess-f} is the droop parameter with the slope of $\frac{1}{K_{bess-f}}$. BESS droop characteristics (charging/discharging) can be demonstrated in three operating regions as shown in Fig. 6. The battery storage should consume surplus energy (charging mode) if actual grid frequency $f_{grid} > f_{ch}$ (charging frequency), and delivers (discharging mode) power shortage when $f_{grid} < f_{disch}$ (discharging frequency) according to their droop characteristics. BESS can participate in an energy exchange if battery SOC is available within the defined SOC constraints. The region between f_{ch} (1.003pu) and f_{disch} (0.997pu) is known as non-critical region according to Australian NEM frequency operating standard (deadband) [27] that defines BESS inactive region. The maximum charge power (P_{ch-max}) is activated (if $f_{grid} > f_{ch}$) for a frequency

deviation of Δf_{max} as long as SOC remains lower than maximum SOC as shown in Fig. 6. The maximum discharge power ($P_{disch-max}$) is activated for a frequency deviation of Δf_{min} until battery SOC reaches to the lower limit.
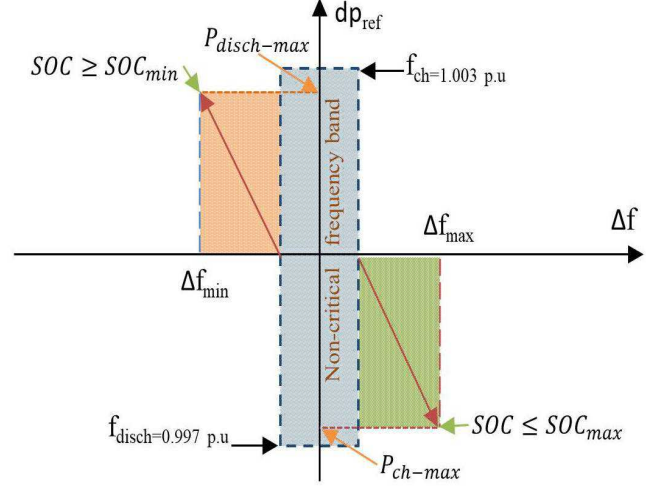

Fig. 6. Frequency droop characteristics

2) Voltage droop controller: The principle of voltage droop controller works in a similar way as in frequency droop controller and can be obtained as in (6) [37]:

$$dq_{ref} = \frac{1}{K_{bess-v}}(v_{ref} - v_{grid}) \tag{6}$$

where, v_{ref} is the voltage reference (steady state voltage in pu), dq_{ref} is the reactive power reference based on reactive power-voltage (Q-V) droop controller, K_{bess-v} is the voltage droop parameter whose slope is $\frac{1}{K_{bess-v}}$. BESS supports reactive power for positive and consumes reactive power for negative dq_{ref} as shown in Fig. 7. The non-critical region (deadband) for voltage control is selected as 0.008pu, with a slope value of 10. The maximum reactive power supply (Q_{max}) is activated (if $v_{grid} < v_{supply}$) for a voltage deviation of Δv_{min} as long as battery converter capacity is available. The maximum reactive power consumption ($-Q_{max}$) is activated (if $v_{grid} > v_{consume}$) for a voltage deviation of Δv_{max} until battery converter capacity reaches to its maximum limit.

3) Active / Reactive Power (PQ) Controller with Lead-lag Controller: The error between active power output at BESS AC terminal and power reference from frequency droop controller in d axis and Δi_d from charge controller generates active power reference signal utilizing first-order filter and a lead-lag controller whereas reactive power reference is generated by associated reactive power measurements in q axis and Δi_q from charge controller. A lead-lag type phase compensator is used in PQ controller to provide necessary filtering and phase shift. In a lead controller, the zeros are placed closer to the origin compared to the poles whereas in a lag controller, the poles are placed closer to the origin compared to the zeros. A lead-lag controller combines the
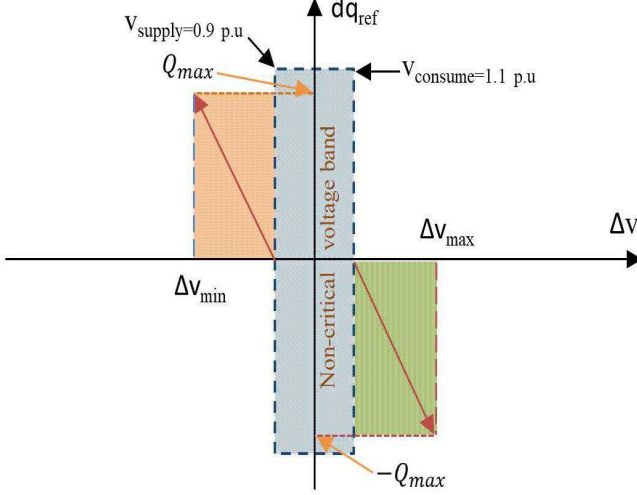
Fig. 7. Voltage droop characteristics

benefits of individual controller to provide value-added performance in system stability by reducing steady state error and settling time. The limiter in lead-lag controller defines the boundary of power reference which is normally within the maximum capacity of BESS converter rating. The typical procedures of poles/zeros placing are discussed in [38], [39]. The transfer functions with calculated poles/zeros locations of lead-lag controller to generate active power reference can be written as in (7):

$$K_d(s) = \frac{T_3}{T_4}\frac{(s+z_1)}{(s+p_1)}\frac{T_5}{T_6}\frac{(s+z_2)}{(s+p_2)} \qquad (7)$$

The transfer functions with calculated pole/zero locations of lead-lag controller to generate reactive power reference can be defined as in (8):

$$K_q(s) = \frac{T_9}{T_{10}}\frac{(s+z_3)}{(s+p_3)}\frac{T_{11}}{T_{12}}\frac{(s+z_4)}{(s+p_4)} \qquad (8)$$

where, $T_3 > T_4$, $T_9 > T_{10}$ for lead controller and $T_5 < T_6$, $T_{11} < T_{12}$ for lag controller. The associated parameters are $T_3=T_9=40$ $T_4=T_{10}=38$, $T_5=T_{11}=13$, $T_6=T_{12}=35$, $z_1=z_3=0.025$, $p_1=p_3=0.026$, $z_2=z_4=0.077$, $p_2=p_4=0.028$, Kp=2.1, Kq=0.1, $T_1=T_2=T_7=T_8=5$.

D. BESS Control and Battery Charge/Discharge Management

BESS provides oscillation damping by absorbing excess and supplying shortfall of energy during transient oscillations to mitigate temporary power deficit. Fig. 6 illustrates the noncritical frequency boundary $\Delta f=\pm$ 150mHz i.e. BESS inactive window for primary frequency control. In a 50Hz (1pu) system, full BESS power is activated for a frequency deviation of 0.2Hz (0.004pu) to preserve power system stability by reducing generation-demand imbalances. The available primary power is linearly activated according to P-f droop characteristics as shown in (3). When the frequency changes beyond the deadband window, BESS current flows in opposite

direction of frequency change. Nevertheless, battery charging or discharging is controlled by battery SOC as shown in Fig. 8.

In comparison to single-level SOC max/min limit to maintain battery SOC [19], a new two-level adaptive charging SOC strategy is proposed in this study i.e a combination of conventional droop-type charging maximum SOC and a new adaptive charging SOC threshold. The main advantage of the proposed two-level (SOC_{max} or adaptive SOC) adaptive charging strategy is that, any recharging SOC limit can be selected by simply changing the value of charging current and therefore, offers additional degree of charging flexibility according to the adaptive planning of BESS operator for battery recharging.

1) BESS With Droop-type Charging/Discharging: Without additional charging mechanism, classical BESS charging/discharging is regulated automatically according to the P-f droop characteristics. BESS is designed to supply active power, if battery SOC is greater than or equal to the minimum SOC i.e. 0.2pu and absorb active power, if SOC is less than or equal to the maximum SOC i.e. 1 per unit. Therefore, overall droop-type charging/discharging strategy can be defined as in (9)

$$i_{d-in} = \begin{cases} i_{d-ref} & SOC \geq SOC_{min} \\ -i_{d-ref} & SOC \leq SOC_{max} \\ 0 & \text{otherwise} \end{cases} \qquad (9)$$

The maximum current calculation of the converter is calculated as in (8) and (9):

$$i_{d-ref-out} = \int_{-|maxValue|}^{|maxValue|} i_{d-in}\ dt \qquad (10)$$

$$i_{q-ref-out} = \int_{-y_{value}}^{y_{value}} i_{q-in}\ dt \qquad (11)$$

where, $y_{value}=\sqrt{\left|\int_0^{|maxValue|^2}|maxValue|^2 - i_{d-in}^2\right|}$ and max= maxValue=1.

BESS droop-type charging/discharging according to the P-f characteristics has significant domination on the availability of necessary battery capacity. At post fault equilibrium point, depending on the level of active power exchanges, SOC of the battery will change (decrease/increase). In addition, as a result of limited efficiency, battery self-discharges over the inactive period. This requires over-sizing the capacity of BESS to avoid reaching minimum SOC and hence increases expenses that reduces system profitability.

2) BESS Charging with Maximum SOC: If SOC decreases lower than a certain limit (may not be at minimum SOC), the resolution is to restore battery SOC to the maximum SOC of 1 pu using small recharge current within the non-critical frequency region or when active power reference current is very small. This ensures that adequate BESS capacity is
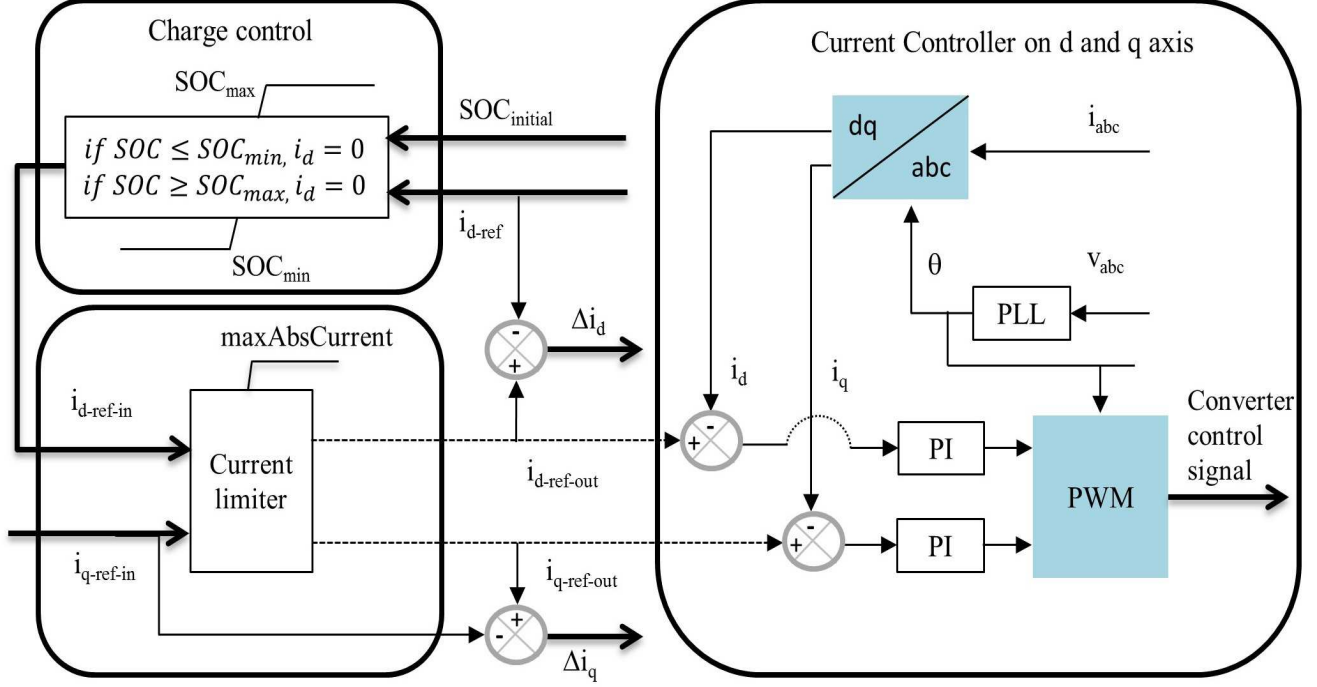
Fig. 8. The block diagram of BESS charge controller, d and q axis current control

available to participate in the next possible contingency event. The adopted recharging strategy can be defined as in (12)

$$
i_{d-in} = \begin{cases} i_{ch-cur} & \text{if SOC} \le (SOC_{min} + SOC_{max})/2 \text{ or} \\ & \text{SOC} \le SOC_{min} \text{ and } i_{d-ref} < 0.0001 \\ 0 & \text{otherwise} \end{cases}
$$
(12)

where, i_{ch-cur} is the charging current when active current reference on d axis is less than 0.0001pu and SOC is lower than 0.5 or at SOC_{min}. Practically, BESS current reference does not settle down to zero completely due to converter losses and battery self-discharge etc. Therefore, recharging current is designed to act when active current reference is less than 0.0001pu. The recharging current of 0.01pu flows before battery reaches to the maximum SOC.

3) BESS Charging with Adaptive SOC: If the battery is recharged to the maximum SOC, BESS loses the ability to participate in any over-frequency event to absorb excess power. Therefore, a separate SOC limit for adaptive charging is proposed to control BESS energy level within the operators' defined window to preserve some frequency margin for over-frequency event without affecting classical droop-type charging/discharging or maximum SOC ceiling. In charging with adaptive SOC, battery charging starting point is same as in *BESS Charging with Maximum SOC*. Adaptive SOC limit is regulated by the value of charging current. The limit of SOC changes to the adaptive SOC limit (defined by BESS operator) if charging current is greater than the SOC switching threshold.

The swapping logic of SOC can be written as in (13)

$$
SOC_{max} = \begin{cases} SOC_{adaptive} & \text{if } i_{rch-cur} > i_{ch-threshold} \\ maxSOC & \text{if } i_{rch-cur} \le i_{ch-threshold} \end{cases}
$$
(13)

The selected value for $i_{ch-threshold}$ is 0.1pu. Therefore, a recharging current of 0-0.1pu implies SOC_{max} of 1 pu. The selected recharging current $i_{rch-cur}$ is 0.015pu for charging with adaptive SOC and the value of $SOC_{adaptive}$ is 0.8pu. Both the charging threshold and charging current can be adjusted according to the planning of BESS operator.

E. Current Controller on d and q axis

The current controller reference in d and q axis ($i_{(d-ref-out)}$ and $i_{(q-ref-out)}$) are attained from BESS damping controller and the measured d and q axis current signal of converter's AC are the inputs to the current controller. The pulse width modulation p_{md} and p_{mq} output at current controller is transformed using phase-locked-loop (PLL) to give reference phase angle and same reference to regulate DC/AC converter.

IV. ATTRIBUTES OF THE TEST SYSTEM

The impact of PV penetration in operating frequency are investigated on IEEE 9-bus system as shown in Fig. 9 [40].

The dynamic model of generators are considered as SG1 (Hydro) which is the reference machine, SG2 (Gas turbine), SG3 (Coal plant) and the network modeling details are available in [41]. The generators are equipped with governor and automatic voltage regulator (AVR). The aggregated PV is connected to the network via 0.6/230kV step-up transformer

at bus 9 and the corresponding information of detailed PV modeling is available in [28]. BESS AC side voltage rating is 0.4kV and linked to the network at bus 7 through 0.4/230kV step-up transformer. The existing coal based SG3 unit is replaced by the aggregated PV system considering sustainable energy initiative to close down fossil fueled power plants. The purpose of BESS installation is to provide additional damping and enhance transient responses to comply with the grid requirements.

A. Case Studies

Two types of generator operating strategies are considered to investigate PV penetration impact. Strategy 1 in Table I defines 100MW PV penetration with nominal operation of synchronous generators. The increment of both generator's output due to permanent load growth is reflected in strategy 2 that replicates the circumstance when selecting convenient generator output option is not available to meet higher load demand.

To understand different aspects of stability challenges induced by PV penetration and demonstrate the proposed SOC recovery strategy, four cases are considered with and without BESS as follows:

- Case 1: Line outage event with-
    - (a) Operating strategy 1
    - (b) Operating strategy 2
- Case 2: Load event with Operating strategy 1
- Case 3: BESS installation location and Converter sizing
    - (a) Operating strategy 2 for line loss
    - (b) Operating strategy 1 for load event
- Case 4: Battery recharging with Operating strategy 1
- Case 5: The operational flexibility and comparative advantages of the proposed adaptive SOC recovery
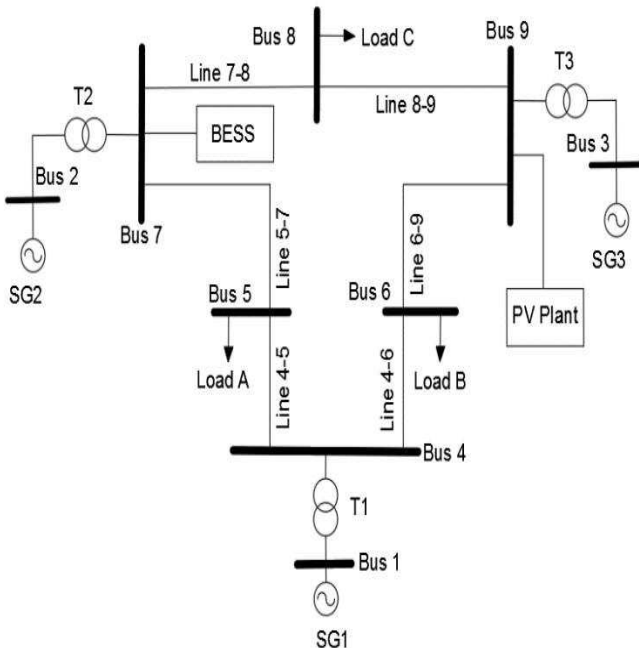

Fig. 9. The IEEE 9-bus system with PV and BESS location

TABLE I
ACTIVE POWER OF GENERATORS AND LOADS IN MW WITH DIFFERENT GENERATOR OPERATING STRATEGIES

Strategy	SG1	SG2	PV	Load A	Load B	Load c
Strategy 1	86	140	100	125	90	100
Strategy 2	107	165	100	150	110	100

V. ANALYSIS OF TRANSIENT STABILITY

The transient analysis is carried out for two contingency scenarios i.e. permanent line outage and load events to investigate inertial impact of PV and the control of conventional synchronous generator to maintain grid operating frequency standards and assimilate BESS to ensure successful power system operation within the grid constraints. In addition, the installation location of BESS and the size of BESS converter are also investigated in maintaining grid operating standards.

A. Line outage event - Case 1

Line outage occurs quite often as a result of fault on the line or structural damages of electric poles. The line 5-7 and line 8-9 are considered to investigate systems' transient behavior in accordance with the grid operating standards. A single-phase-to-ground fault is applied on line 5-7 and line 8-9 at t=0s. The fault on line 5-7 is cleared and restored after t=0.24s and the fault on line 8-9 is cleared by removing the line permanently. With a single-phase-to-ground fault, the system may experience instability if sufficient oscillation damping is not provided by the generator excitation systems. A power system stabilizer (PSS) is often used to provide additional system damping to resolve instability phenomena.

The simulation results as shown in Fig. 10 illustrates that without any PV penetration (w/strategy 1 & w/out PV and w/strategy 2 & w/out PV), the deviations in frequency oscillation remain within the NEM defined regulatory boundary for both the operating strategies 1 and 2. Nevertheless, with 100MW PV penetration, the frequency oscillations with operating strategy 1 (Case 1 (a)(w/strategy 1 & PV and w/strategy 1,PV & PSS) also remains within the grid defined $\pm2\%$ of the nominal value. The synchronous generators have greater margin in regulating active power output and this defines the damping capability of the existing power system to maintain frequency stability without any energy storage system for line outage events. Nonetheless, the maximum frequency deviation increases by 0.275Hz for SG1 and 0.115Hz for SG2 with 18.18% PV penetration than without PV plant condition when operating strategy 1 is selected as shown in Table II.

However, in the case of permanent increase in load demand, generators are required to operate at higher output that resembles operating strategy 2 (Case 1 (b)). The post fault position in Fig. 10, with operating strategy 2 (w/strategy 2 & PV) illustrate that frequency responses are quite oscillatory and violate the grid operating standards with and without a PSS, due to insufficient damping capability of generators excitations system. Table II demonstrates that the maximum frequency oscillation of generators SG1 and SG2 rises with the increased PV penetration. Although PSS provides some degree
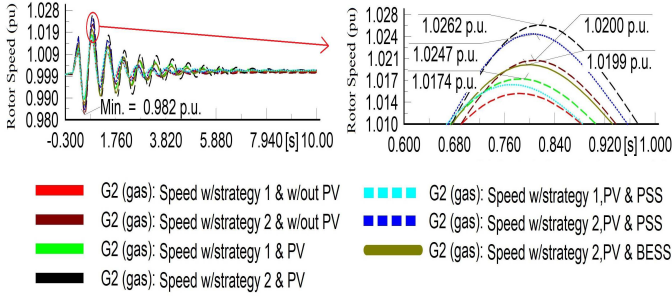
8

Fig. 10. The frequency (pu) oscillations of generator G2

Fig. 11. Voltage at BESS connection point

Fig. 12. The active and reactive power of BESS and battery SOC

of damping support that reduces the impact of PV penetration marginally (w/strategy 2,PV & PSS), but grid frequency standard is not maintained due to insufficient damping provided by the PSS.

TABLE II
MAXIMUM FREQUENCY DEVIATION UNDER DIFFERENT OPERATING
STRATEGIES AND GENERATION SCENARIOS

Operating Strategy	W/out PV	With PV	PV & PSS	PV & BESS	Generator
Strategy 1	1.009	1.0134	1.0129	-	SG1
Strategy 2	1.0148	1.0203	1.0196	1.0155	
Strategy 1	1.0151	1.0174	1.0165	-	SG2
Strategy 2	1.0200	1.0262	1.0247	1.0199	

Therefore, a 35MW BESS (BESS converter size) is installed at bus 7 to provide additional damping to retain frequency oscillation within the defined grid constraints according to their droop setting characteristics (w/strategy 2,PV & BESS). The system responses in Fig. 10 settle down to their original steady-state position faster than a system without BESS by providing adequate oscillation damping and this demonstrates better transient performance than that of with and without conventional PSS controller. This signifies the importance of BESS in mitigating PV penetration impact on power system frequency control and fulfilling mandatory grid requirements according to NEM frequency regulatory framework.

In addition, BESS not only enhances the transient frequency responses but also reduces active power oscillation of synchronous generators than that of a system without BESS/PSS. The voltage at BESS connection point in Fig. 11 illustrates that BESS reduces voltage drop during the fault periods and likewise diminishes voltage oscillations faster compared to other circumstances.

Fig. 12 shows the variation in battery SOC for both energy surplus and shortage states during frequency deviation and BESS power output. The figures (Figs. 10 and 12) reveal that to comply with the grid frequency operating standards, larger converter size and smaller energy capacity is required as additional damping support is needed only for a short period of time. The selected battery capacity is 180kWh considering all the case studies, however, authors do not claim that this is an optimal BESS energy capacity.
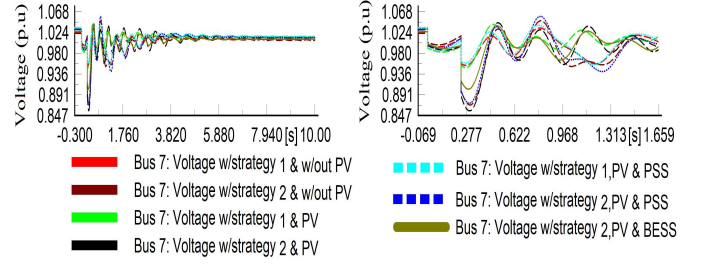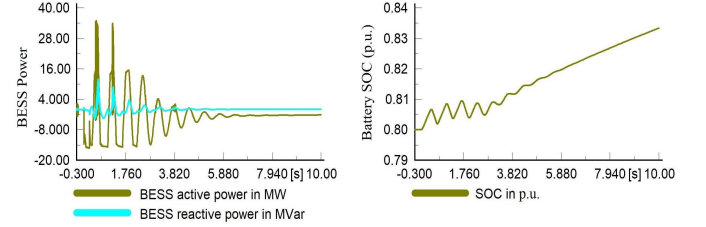
B. Load Event Scenario - Case 2

A sudden increase or decrease in load demand at any particular buses can initiate system transients that are essential to be resolved through sufficient system damping. The aforementioned case study of line outage event shows that with operating strategy 1, the system responses oscillate within the frequency operating boundary and therefore the same strategy is selected to investigate, if the system remains effective in maintaining similar level of stability achievement in the case of load event. The performance of the 9-bus system is investigated with a 50% load reduction event at load A (load value reduces from 125MW to 62.5MW) for the period of t=0-0.6s when operating strategy 1 is chosen. The simulation results of load event in Fig. 13 shows that without any PV penetration (w/strategy 1 & w/out PV), the generators are able to maintain the grid defined frequency boundary of ±1% of the nominal value for load event. However, with integrated PV, generator excitations system and with or without PSS controller (w/strategy 1 & w/PV and w/strategy 1,PV & PSS) fails to deliver necessary damping to mitigate oscillatory transient (acceleration/deceleration) system responses that are originated due to load change.

Therefore, a 35MW BESS is installed at bus 7 to provide additional damping and reduce frequency oscillation. The frequency response of generator SG1 illustrated in Fig. 13 manifests that BESS provides sufficient oscillation damping and post-fault frequency response is recovered effectively within the grid frequency boundary.

BESS active and reactive power and alternating battery SOC with grid frequency variation are shown in Fig. 14 which demonstrates that larger BESS converter size is the prerequisite than larger BESS energy capacity. The simulation studies also reveal that incorporated BESS not only decreases oscillatory behavior of the system but also reduces active
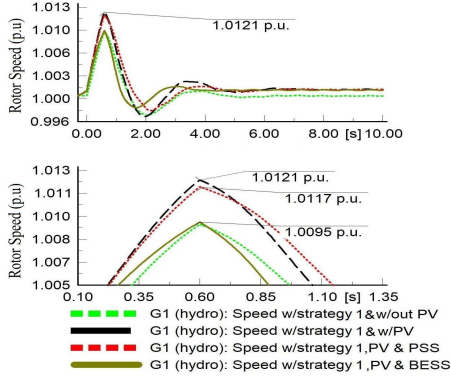
Fig. 13. The frequency (pu) oscillation of generator G1 with load event

power and transient voltage oscillation and stabilizes faster than PSS.
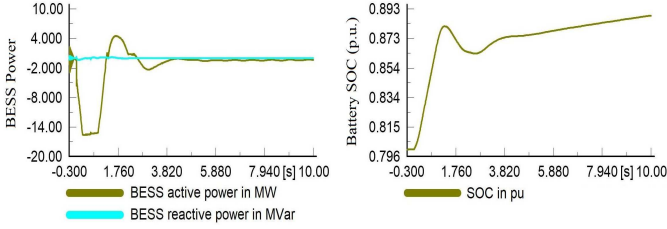

Fig. 14. The active and reactive power of BESS and battery SOC

C. BESS Installation Location and Converter Sizing - Case 3

The location of BESS installation is very important to ensure the best performance of BESS while utilizing the smaller BESS converter size and battery energy capacity that in turn reduces the costs associated with BESS, power losses and increases benefits to the system. Therefore, the proposed lead-lag based BESS is installed at different buses to investigate BESS performance. However, it is worth noting that optimal battery energy capacity is not considered in this paper. The approach of finding a suitable BESS installation location is based on comparative performance analysis when BESS is installed at different high-voltage buses undergoing loss of line with operating strategy 2 and load event with operating strategy 1. The converter size is determined considering the minimum BESS converter MW rating to maintain the frequency within the grid defined frequency regulatory requirements when BESS is installed at different buses for the studied operating strategies and contingencies. It is perceived that in the case of large system, installing BESS at all buses is not a feasible technique and therefore optimization algorithm need to be adopted which is out of the scope of this study. Hence, this study is limited to trial and error based method to find optimal location and size to provide primary frequency control. The simulation results of line-outage event and BESS with 35MW rated converter (w/strategy 2,PV & BESS) installed at different buses in Fig. 15 illustrates that not all the location with the rated BESS capacity become successful to comply with the grid constraints. It is evident

that BESS at bus 7 ensures the best performance of BESS compared to any other location for all the studied cases and strategies.
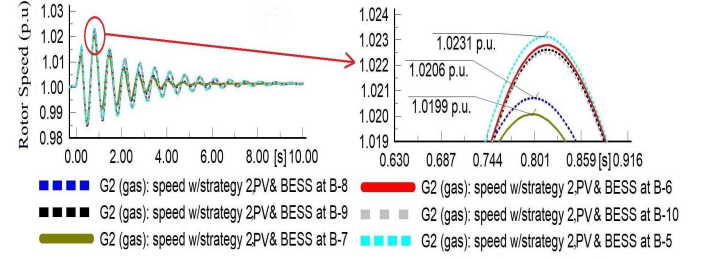

Fig. 15. Generator frequency with BESS installed at different buses

On the contrary, load event scenario with operating strategy 1 (w/strategy 1,PV & BESS) demonstrates similar performance and BESS installed at bus 7 complies efficiently with the grid operating standards regardless of the installation location. Therefore, it can be concluded that bus 7, closer to the generator SG2, is the best location to obtain the most benefit of BESS installation concerning studied contingencies. Moreover, this also indicates that BESS near generator terminal is much effective in maintaining frequency operating standard in case of disturbance events.

D. Battery recharging with the proposed method - Case 4

A new two-level battery charging strategy is proposed in this study. Based on adaptive recharging plan, SOC limit during recharging can be adjusted separately than droop-controlled maximum charging end point. A 42% load increase event is applied for the duration of t=0-0.8s at load A when the grid is operating with strategy 1 to demonstrate different scenarios with and without the proposed SOC recovery strategy. The battery is rated as 20Ah and 0.9kV. Initial SOC=0.8 pu, internal resistance (Ω)=0.001 pu. SOC at different charging strategies are illustrated in Fig. 16. Fig. 16 shows that without battery recharging, SOC is lower than 0.6pu. Therefore, according to the proposed recharge strategies, battery is recharged based on the value of charging current. Fig. 16 exhibits that when battery is charged using a recharging current of 0.015pu, maximum defined SOC ceiling is selected as 0.8pu and with a recharging current of 0.10pu, maximum SOC threshold is 1pu.
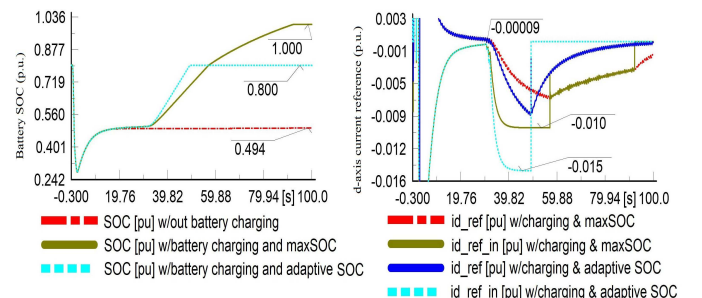

Fig. 16. SOC status with different charging mechanism

Simulation results in the figure illustrates that recharging action takes place at the point of active current reference lower than 0.0001pu. This validates the efficacy of the proposed two-level charging SOC limits that ensures flexible BESS charging strategy defined by the BESS operator. The charging time from network event is approximately 30.5s (starts at t=0s and ends at t=30.5s). The recharging time for maxSOC is approximately 62.1s (starts at t=30.5s and ends at t=92.6s) and for adaptive SOC is 18.6s (starts at t=30.5s and ends at t=49.1s). This charging and recharging time may vary according to battery charging current, battery energy capacity, SOC limit and network conditions.

E. The operational flexibility and comparative advantages of the proposed adaptive SOC recovery - Case 5

A temporary 45% load increase event is applied for the duration of t=0-0.8s at load A when the grid is operating with strategy 2 to demonstrate different scenarios with and without the proposed SOC recovery strategy. The battery is rated as 7.8Ah and 0.9kV. Based on load/generation forecast, the BESS operator can select an appropriate SOC limit for the possible upcoming discharge or charge scenarios. For example, according to weather forecast, a cloud-passing is expected over the PV farm in the next hour, hence battery can be recharged to 1pu to ensure the maximum availability of BESS capacity for reduced PV generation and mitigate PV impact on the grid frequency. The PV output power is reduced from 100MW to 90MW at t=42s, 73MW at t=50s, further reduced to 68.3MW at t=60s and finally returned to initial 100MW at t=70s. The simulation results shown in Fig. 17 illustrate that without a BESS, frequency nadir is lower than the grid defined value and with the integrated BESS minimum frequency remains within the grid constraint. On the contrary, it can be seen in Fig. 18 (a) that BESS provides better voltage regulation compared with the case of without a BESS. Fig. 18 (b) shows BESS active and reactive power contribution during the total simulation periods. Battery is recharged when BESS is in the inactive region between 31-39s. As expected, adaptive SOC value equal to 1pu takes a longer time to recharge than the adaptive SOC value of 0.9pu. Battery recharging periods are 3.95s (SOC=0.8pu) and 6.32s (1pu) for a charging current of 0.012pu and 0.10pu respectively.

The simulation results in Fig. 19 (a) shows that higher SOC is available at the end of the reduced PV generation periods if the battery is recharged to maximum SOC level prior to the contingency events (adaptive SOC=1.00 [pu]) compared to lower SOC value (adaptive SOC=0.8 [pu]). Similarly, if PV peak generation is expected i.e. in the midday, battery can be recharged upto 0.8pu to consume surplus PV energy.

In addition to operational flexibility, Fig. 19 (b) shows the comparative advantage of the proposed SOC recovery than the conventional SOC recovery methods. Fig. 19 (b) manifests that the recharging SOC can be adjusted to 0.8pu or 1pu based on the planning of the BESS operator. However, this does not restrict the maximum SOC limit (1pu) during a network event (a temporary 25% load reduction at load A during t=0-0.8s with operating strategy 2). With adaptive
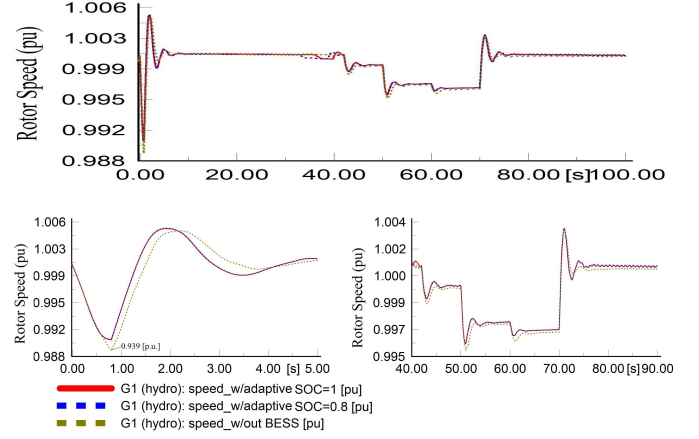

Fig. 17. The frequency of generators [p.u.] and voltage oscillations [p.u.] at bus and PCC with BESS (a) and responses with PI, PI-lead and lead-lag controlled BESS (b)
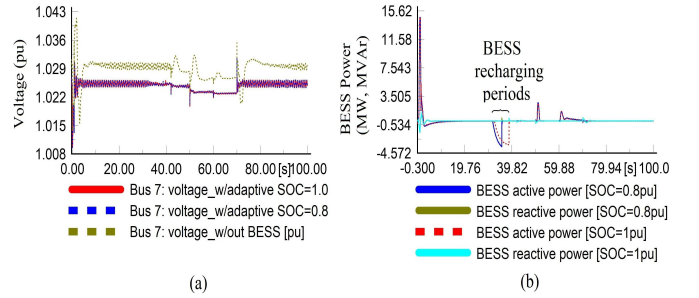

Fig. 18. Voltage at BESS connection point (a) and BESS active/reactive power (b)

Fig. 19. SOC status with different charging mechanism

SOC recovery, battery can consume surplus energy until SOC reaches to 1pu and thus allows use of the the maximum BESS capacity for network event (frequency/voltage controller has priority over charging current). In this way, the proposed adaptive SOC recovery provides an unique benefit of adopting a flexible battery SOC management without compromising BESS capacity for network support compared to the existing study in [19]. Thus the ultimate goal of the proposed SOC recovery can be summarized as follows:

- Battery SOC can be recharged to a value lower than the maximum SOC considering the forecast of peak PV generation in the next hour.
- Battery SOC can be recharged to the maximum SOC con-

sidering the forecast of reduced PV generation/increased load demand in the next hour.

- While recharged SOC can be adjusted to a different value according to the BESS operators' plan, this does not reduce the maximum SOC value when responding to an unexpected network event.

VI. Conclusion

A droop-type, lead-lag controlled BESS with novel SOC recovery strategy is proposed to provide additional damping and enhance the primary frequency response of the system with increased PV penetration level in the power system. The adaptive SOC recovery aims to provide better flexibility for BESS energy management planning based on PV forecast in comparison to classical droop-type charging for future transient events. The presented study can be summarized as follows:

- The network performance largely depends on how synchronous generators are being operated before the contingency period. Available headroom diminishes during peak time or reduction in PV farm output and forces synchronous generators to be operated at higher output.
- Simulation studies demonstrate that according to NEM criteria, the system responses violate grid frequency regulation with and without a PSS when PV penetration increases.
- Nevertheless, incorporating BESS effectively regulates and damps out system oscillations by providing additional system damping. Therefore, it is evident that BESS has the capability to mitigate inertia related negative impacts of PV, satisfy grid regulations and thus can avoid penalty for regulation violation.
- Also, BESS enhances transient voltage profile of the system.
- Moreover, BESS converter size is more crucial than BESS energy capacity as the primary frequency is required for a few seconds only. It is also observed that, BESS near the generator terminal provides better benefit in term of fulfilling grid regulation.
- Furthermore, the proposed adaptive SOC recovery allows to obtain flexible recharging SOC level in accordance with BESS operator plan and PV/other forecast and this does not restrict the SOC limit for unexpected network event. This provides the added benefit of flexible operational planning of BESS whenever needed.

The proposed BESS and SOC recovery strategy can be easily adopted in large-scale interconnected power system or small isolated power system which consists of various alternating energy sources through the proper modification of the BESS connection with the grid which provides the wider applicability of the proposed study in terms of stability enhancement and the planning of battery energy management.

With sustainable energy movements, this research suggests that increasing PV penetration while maintaining power system stability and reliability is possible to achieve by incorporating a BESS that is capable of providing prompt response and thereby enhancing overall system inertia. Increasing the level of PV penetration, their impact on transient frequency stability and new BESS control strategies to enhance system performance will get further attention in future research work.

References

[1] International Energy Agency, "Renewables 2017, [Available Online]: https://www.iea.org/publications/renewables2017, [Accessed on: 2018-07-01]."

[2] P. Du and Y. Makarov, "Using disturbance data to monitor primary frequency response for power system interconnections," *IEEE Transactions on Power Systems*, vol. 29, no. 3, pp. 1431–1432, May 2014.

[3] S. Eftekharnejad, V. Vittal, G. T. Heydt, B. Keel, and J. Loehr, "Small signal stability assessment of power systems with increased penetration of photovoltaic generation: A case study," *IEEE Transactions on Sustainable Energy*, vol. 4, no. 4, pp. 960–967, Oct 2013.

[4] R. Shah, N. Mithulananthan, and R. Bansal, "Oscillatory stability analysis with high penetrations of large-scale photovoltaic generation," *Energy Conversion and Management*, vol. 65, pp. 420 – 429, 2013, Global Conference on Renewable Energy and Energy Efficiency for Desert Regions 2011 GCREEDER 2011.

[5] S. You, G. Kou, Y. Liu, X. Zhang, Y. Cui, M. J. Till, W. Yao, and Y. Liu, "Impact of high PV penetration on the inter-area oscillations in the u.s. eastern interconnection," *IEEE Access*, vol. 5, pp. 4361–4369, 2017.

[6] R. Shah, N. Mithulananthan, and K. Y. Lee, "Large-scale PV plant with a robust controller considering power oscillation damping," *IEEE Transactions on Energy Conversion*, vol. 28, no. 1, pp. 106–116, Mar 2013.

[7] D. Remon, A. M. Cantarellas, J. M. Mauricio, and P. Rodriguez, "Power system stability analysis under increasing penetration of photovoltaic power plants with synchronous power controllers," *IET Renewable Power Generation*, vol. 11, no. 6, pp. 733–741, 2017.

[8] D. Remon, C. A. Cañizares, and P. Rodriguez, "Impact of 100-mw-scale PV plants with synchronous power controllers on power system stability in northern chile," *IET Generation, Transmission Distribution*, vol. 11, no. 11, pp. 2958–2964, 2017.

[9] L. Zhou, X. Yu, B. Li, C. Zheng, J. Liu, Q. Liu, and K. Guo, "Damping inter-area oscillations with large-scale PV plant by modified multiple-model adaptive control strategy," *IEEE Transactions on Sustainable Energy*, vol. 8, no. 4, pp. 1629–1636, Oct 2017.

[10] H. Xin, Y. Liu, Z. Wang, D. Gan, and T. Yang, "A new frequency regulation strategy for photovoltaic systems without energy storage," *IEEE Transactions on Sustainable Energy*, vol. 4, no. 4, pp. 985–993, Oct 2013.

[11] Z. Jietan, Q. Linan, R. Pestana, L. Fengkui, and Y. Libin, "Dynamic frequency support by photovoltaic generation with "synthetic" inertia and frequency droop control," in *2017 IEEE Conference on Energy Internet and Energy System Integration (EI2)*, Nov 2017, pp. 1–6.

[12] V. A. K. Pappu, B. Chowdhury, and R. Bhatt, "Implementing frequency regulation capability in a solar photovoltaic power plant," in *North American Power Symposium 2010*, Sep 2010, pp. 1–6.

[13] S. I. Nanou, A. G. Papakonstantinou, and S. A. Papathanassiou, "A generic model of two-stage grid-connected PV systems with primary frequency response and inertia emulation," *Electric Power Systems Research*, vol. 127, pp. 186 – 196, 2015. [Online]. Available: http://www.sciencedirect.com/science/article/pii/S0378779615001868

[14] N. Nguyen and J. Mitra, "An analysis of the effects and dependency of wind power penetration on system frequency regulation," *IEEE Transactions on Sustainable Energy*, vol. 7, no. 1, pp. 354–363, Jan 2016.

[15] Australian Energy Market Operator (AEMO), "Schedule of Constraint Violation Penalty Factors, [Available Online]: https://www.aemo.com.au/-/media/Files/Electricity/NEM/Security_and_Reliability/Congestion-Information/2016/Schedule-of-Constraint-Violation-Penalty-factors.pdf, [Accessed on: 2018-12-24]."

[16] A. Oudalov, D. Chartouni, and C. Ohler, "Optimizing a battery energy storage system for primary frequency control," *IEEE Transactions on Power Systems*, vol. 22, no. 3, pp. 1259–1266, Aug 2007.

[17] R. Shah, N. Mithulananthan, and R. Bansal, "Damping performance analysis of battery energy storage system, ultracapacitor and shunt capacitor with large-scale photovoltaic plants," *Applied Energy*, vol. 96, pp. 235 – 244, 2012.

[18] M. R. Aghamohammadi and H. Abdolahinia, "A new approach for optimal sizing of battery energy storage system for primary frequency control of islanded microgrid," *International Journal of Electrical Power and Energy Systems*, vol. 54, pp. 325 – 333, 2014.

[19] P. Mercier, R. Cherkaoui, and A. Oudalov, "Optimizing a battery energy storage system for frequency control application in an isolated power system," *IEEE Transactions on Power Systems*, vol. 24, no. 3, pp. 1469–1477, Aug 2009.

[20] U. Datta, A. Kalam, and J. Shi, "Battery energy storage system to stabilize transient voltage and frequency and enhance power export capability," *IEEE Transactions on Power Systems*, pp. 1–1, 2018.

[21] G. Xu, L. Xu, and J. Morrow, "Power oscillation damping using wind turbines with energy storage systems," *IET Renewable Power Generation*, vol. 7, no. 5, pp. 449–457, Sep. 2013.

[22] D. Zhu and Y. A. Zhang, "Optimal coordinated control of multiple battery energy storage systems for primary frequency regulation," *IEEE Transactions on Power Systems*, vol. 34, no. 1, pp. 555–565, Jan 2019.

[23] Q. Xu, J. Xiao, P. Wang, X. Pan, and C. Wen, "A decentralized control strategy for autonomous transient power sharing and state-of-charge recovery in hybrid energy storage systems," *IEEE Transactions on Sustainable Energy*, vol. 8, no. 4, pp. 1443–1452, Oct 2017.

[24] J. Xiao, P. Wang, and L. Setyawan, "Hierarchical control of hybrid energy storage system in dc microgrids," *IEEE Transactions on Industrial Electronics*, vol. 62, no. 8, pp. 4915–4924, Aug 2015.

[25] Q. Xu, J. Xiao, X. Hu, P. Wang, and M. Y. Lee, "A decentralized power management strategy for hybrid energy storage system with autonomous bus voltage restoration and state-of-charge recovery," *IEEE Transactions on Industrial Electronics*, vol. 64, no. 9, pp. 7098–7108, Sep. 2017.

[26] AEMC, "The Frequency Operating Standard stage one final-for-publi, [Available Online]: https://www.aemc.gov.au/sites/default/files/content/ce48ba94-b3a9-4991-9ef9-e05814a78526/REL0065-Review-of-the-Frequency-Operating-Standard-Final-for-publi.pdf, [Accessed on: 2018-07-15]."

[27] AEMO, "Generator Technical Requirements, [Available Online]: https://www.aemo.com.au/-/media/Files/Electricity/NEM/Security_and_Reliability/Reports/2017/AEMO-GTR-RCP-110817.pdf, [Accessed on: 2018-07-15]."

[28] DigSILENT GmbH, "PV system," 2017.

[29] P. Shen, M. Ouyang, X. Han, X. Feng, L. Lu, and J. Li, "Error analysis of the model-based state-of-charge observer for lithium-ion batteries," *IEEE Transactions on Vehicular Technology*, vol. 67, no. 9, pp. 8055–8064, Sep. 2018.

[30] Q. Wu, R. Guan, X. Sun, Y. Wang, and X. Li, "SoC balancing strategy for multiple energy storage units with different capacities in islanded microgrids based on droop control," *IEEE Transactions on Sustainable Energy*, vol. 8, no. 4, pp. 1443–1452, Oct 2017.

[31] X. Lu, K. Sun, J. M. Guerrero, J. C. Vasquez, and L. Huang, "State-of-charge balance using adaptive droop control for distributed energy storage systems in dc microgrid applications," *IEEE Transactions on Industrial Electronics*, vol. 61, no. 6, pp. 2804–2815, June 2014.

[32] W. Huang and J. A. A. Qahouq, "Energy sharing control scheme for state-of-charge balancing of distributed battery energy storage system," *IEEE Transactions on Industrial Electronics*, vol. 62, no. 5, pp. 2764–2776, May 2015.

[33] H. Chaoui and C. C. Ibe-Ekeocha, "State of charge and state of health estimation for lithium batteries using recurrent neural networks," *IEEE Transactions on Vehicular Technology*, vol. 66, no. 10, pp. 8773–8783, Oct 2017.

[34] P. Shen, M. Ouyang, L. Lu, J. Li, and X. Feng, "The co-estimation of state of charge, state of health, and state of function for lithium-ion batteries in electric vehicles," *IEEE Transactions on Vehicular Technology*, vol. 67, no. 1, pp. 92–103, Jan 2018.

[35] N. Mukherjee and D. De, "A new state-of-charge control derivation method for hybrid battery type integration," *IEEE Transactions on Energy Conversion*, vol. 32, no. 3, pp. 866–875, Sep. 2017.

[36] DIgSILENT GmbH, "BESS application example," 2017.

[37] S. Akkari, J. Dai, M. Petit, and X. Guillaud, "Interaction between the voltage-droop and the frequency-droop control for multi-terminal hvdc systems," *IET Generation, Transmission Distribution*, vol. 10, no. 6, pp. 1345–1352, 2016.

[38] ControlTheoryPro, "PI-Lead Control, [Available Online]: http://wikis.controltheorypro.com/pi-leadcontrol, [Accessed on: 2018-06-13]."

[39] Z. K. Jadoon, S. Shakeel, A. Saleem, A. Khaqan, S. Shuja, Q. Hasan, S. A. Malik, and R. A. Riaz., "A comparative analysis of PID, lead, lag, lead-lag, and cascaded lead controllers for a drug infusion system," *Journal of Healthcare Engineering*, vol. 2017, Jan 2017.

[40] P. M. Anderson and A. A. Fouad, *Power System Control and Stability, 2nd Edition*. New York: IEEE Press, 2003.

[41] DigSILENT, "Digsilent Powerfactory," 2017.

Ujjwal Datta received the Bachelor of Science (Honours) in Electrical and Electronic Engineering from Stamford University, Bangladesh and Msc in Smart Grid with distinction from Tampere University of Technology, Finland. Currently he is continuing studies towards PhD at Victoria University, Melbourne, Australia. His research interests are power system stability, FACTS devices, Battery energy storage system, smart grid, home energy management system, EV and renewable energy system.

Akhtar Kalam Akhtar Kalam is a Professor at Victoria University (VU), Melbourne since 1985 and a former Deputy Dean of the Faculty of Health, Engineering and Science. He is currently the Head of Engineering and Director of Externalization at the College of Engineering and Science, VU. He is also the current Chair of the Academic Board and lectures in the Masters by coursework program in the Engineering Institute of Technology, Perth, Australia. Again he is the Editor in Chief of Australian Journal of Electrical & Electronics Engineering. Further he has Distinguished Professorship position at the University of New South Wales, Sydney, Australia; MRS Punjab Technical University – Bhatinda, India; Crescent University – Chennai, India; VIT – Vellore, India and 5 Malaysian universities. He has wide experience in educational institutions and industry across four continents. He received his B.Sc. and B.Sc. Engineering from Calcutta University and Aligarh Muslim University, India. He completed his MS and Ph.D. at the University of Oklahoma, USA and the University of Bath, UK. His major areas of interests are power system analysis, communication, control, protection, renewable energy, smart grid, IEC61850 implementation and co-generation systems. He provides consultancy for major electrical utilities, manufacturers and other industry bodies in his field of expertise. Professor Kalam is a Fellow of EA, IET, AIE, a life member of IEEE and a member CIGRE AP B5 Study Committee.

Dr. Juan Shi received the Bachelor of Engineering (Honours) in Electrical Engineering from Northeastern University, China, in 1988 and the PhD degree in Electrical Engineering from Victoria University (VU), Melbourne, Australia, in 1995. Dr Shi received the Graduate Certificate in Tertiary Education from VU in 2003. She joined VU as a Lecturer in 1994, where she is currently an Associate Professor in the College of Engineering & Science. Her current research interests include automatic control and applications, power system stability, intelligent control and applications to smart energy systems, system identification, and engineering education.